A. OLSZÓWKA-MYALSKA*, J. MYALSKI*, M. GODZIERZ*#, P. WRZEŚNIOWSKI*

MAGNESIUM MATRIX COMPOSITE WITH OPEN-CELLED CARBON FOAMS OBTAINED BY POWDER METALLURGY

The preliminary results of the application of open-celled glassy-carbon foam (C_{of}) in magnesium matrix composites processed by the powder metallurgy method were presented. For the component consolidation, compaction with vertically-torsional vibration and hot-pressing were applied. For the material characterization, the microstructure examination LM and SEM with EDS was employed and also, the porosity and microhardness were measured. An influence of the carbon foam cells' size on the composite porosity and microhardness was revealed. Additionally, a generation of a few micrometer thin and differently shaped MgO inclusions was observed. Differences in the oxide phase amount, size and shape in the magnesium matrix measured by the quantitative metallography method in the cross-sectioned composite elements were stated. With an increase of the distance from the composite roller top, an increase of the MgO content and microhardness was noticed.

Keywords: magnesium matrix composites, ceramic-metal interpenetrating composite, open-celled carbon foam, powder metallurgy

1. Introduction

Magnesium matrix composites can be reinforced with ceramic particles (e.g. AlN, Al_2O_3, SiO_2, SiC) [1-5], carbon components in the form of fiber preforms, short fibers and particles, carbon nanotubes [6-9] as well as intermetallic phases (e.g. Mg_2Si, $TiAl_3$) [10-12]. However, only carbon components exhibit density lower than that of magnesium, so their application does not increase the final product's density, while successfully increasing both the mechanical and tribological properties. Magnesium matrix composites reinforced with continuous carbon fibers are proposed for aircraft elements as materials with very high mechanical properties [8]. In case of short carbon fibers application, an increase of mechanical properties and wear resistance are obtained [7], while the glassy carbon particles in magnesium matrix mainly cause a decrease of friction coefficient and mass loss reduction [6].

The application of non-continuous carbon reinforcement, such as particles, short fibers and carbon nanotubes, may cause micro and macro segregation of the reinforcements in the final product [5,6]. In the case of composites processed from carbon-magnesium suspensions, segregation occurs due to the differences in the components' density, and the effect of the reinforcing phases' movement is observed. In the microstructure, due to the characteristic crystallization mechanism, cellular distribution of dispersed phases can be formed [5,6]. In powder metallurgy processes, the proper powder granulation, components' volume fraction and powder mixture preparation are the crucial factors ensuring homogenous component distribution.

In this work, a new material concept for magnesium matrix composites is proposed, i.e. the application of inflexible open-celled glassy-carbon foam as the reinforcing phase, instead of the carbon fibers or particles used so far. That foam, also called the reticulated vitreous carbon (RVC), is structured of cells, the walls of which comprise of windows with different sizes and shapes [13-16]. The geometry of the carbon foams can be characterized by the cell and window size, but most commonly, by the value of pores-per-inch denoted as ppi [14,17-18].

For the last few years, the literature has been reporting the application of ceramic foams in metal matrix composites for aluminium. That type of open-celled porous components makes it possible to design the reinforcement arrangement in the composite before the consolidation process and to better predict the final properties. Those materials can be called ceramic-metal interpenetrating composites (IPCs) [19-31].

However, a new problem induced by the use of open-celled foam is the proper method of components' consolidation. Up till now, such casting technologies as gravity casting [19,26-27], centrifugal casting [22] and pressure infiltration [23,30] has been applied for aluminium matrixes with ceramic foams.

The aim of the presented paper was to exhibit the first results of magnesium matrix composite fabrication, where powder metallurgy processes for magnesium powder and glassy-carbon open-celled foam (C_{of}) consolidation were employed. The ex-

*   SILESIAN UNIVERSITY OF TECHNOLOGY, INSTITUTE OF MATERIAL SCIENCE, DEPARTMENT OF MATERIAL SCIENCE AND METALLURGY, 8 KRASIŃSKIEGO STR., 40-019 KATOWICE, POLAND

Corresponding author: marcin.godzierz@polsl.pl

aminations were focused on the structural effects induced by the proposed technological procedure, consisting of vertically-torsional vibration and hot-pressing [32].

2. Materials and methods

In the experiments, magnesium powder (globular, 60-120 μm, Mg ≥ 99%, Sigma Aldrich) and two types of glassy-carbon open-celled foams of similar open porosity 90 %, with 20 ppi (cell size 816,5 ± 248,5 μm) and 80 ppi (cell size 351,5 ± 94 μm) denoted as $C_{of}20$ and $C_{of}80$, fabricated at Silesian University of Technology by pyrolysis of organic precursor, were applied as the raw materials. The micrographs of the applied initial materials are shown in Fig. 1. In the case of C_{of}, it is visible that the relation between the cell size and the window size is similar, independently of the ppi value (Fig. 1b and c). Also, the magnesium powder granulation is suitable for the particle transportation across the foam cells.

The procedure of component consolidation consisted of the following steps [32]:
– Filling of carbon foam discs (previously placed in a graphite crucible) with Mg powder by way of successive pouring and thickening with vertically-torsional vibration,
– Annealing of the crucible with the C_{of}-Mg powder semi-product at 670°C in vacuum in order to melt the metal and wet the carbon,
– Hot uniaxial pressing of the C_{of}-liquid Mg system with the pressure of 5 MPa for metal compaction and improvement of the metal-carbon bonding.

The Mg powder compaction in the cells of glassy carbon foams by the vertically-torsional vibration method consisted of three steps with the parameters shown in Table 1.

TABLE 1

Parameters of vertically-torsional vibration applied for the compaction of Mg powder in C_{of}

	Amplitude [mm]	Time [s]	Frequency [Hz]
Step 1	0.5	600	
Step 2	1.0	300	50
Step 3	1.5	120	

The magnesium particles just after vertically-torsional vibration were examined by SEM and obtained micrographs are shown in Figures 2 and 3. They exhibit the effects occurring on particles surface as debonding of MgO film from magnesium and oxide refining, as well formation in metal a parallel oriented grooves (Fig. 2). Beside of that, a separation effect of
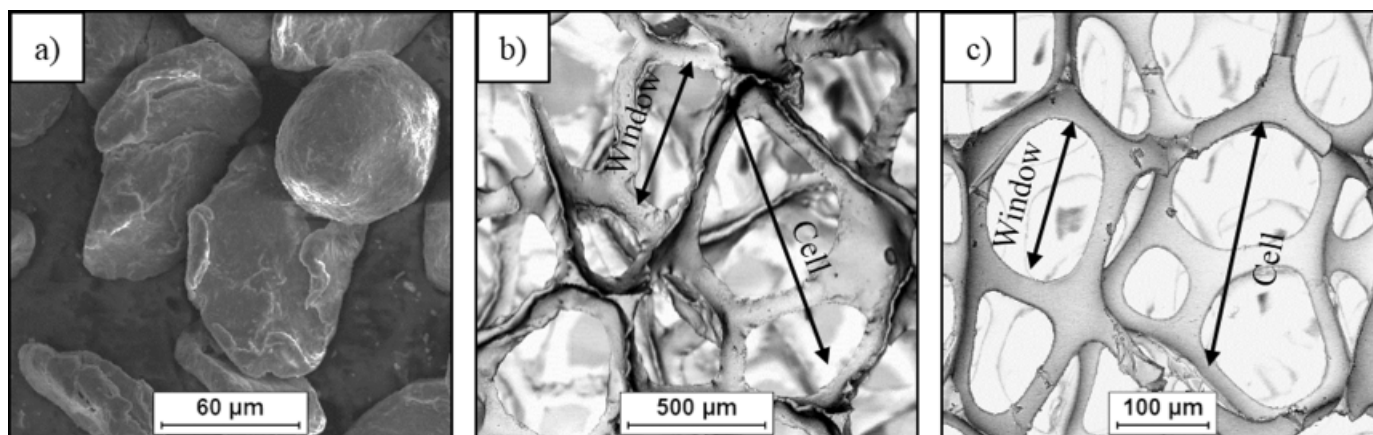

Fig. 1. SEM micrographs of the applied materials: a) magnesium powder, b) $C_{of}20$ and c) $C_{of}80$
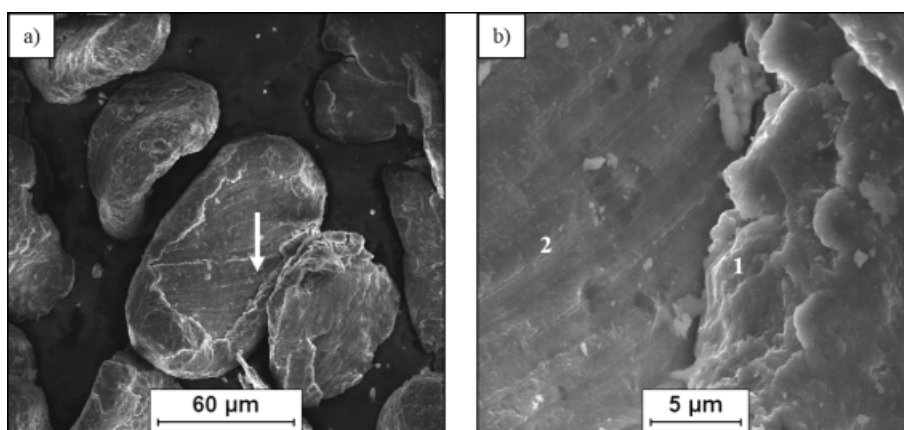

Fig. 2. SEM micrographs of magnesium powder after vertically-torsional vibration, MgO film locally debonded and refined (1), grooves formed at metal surface (2)
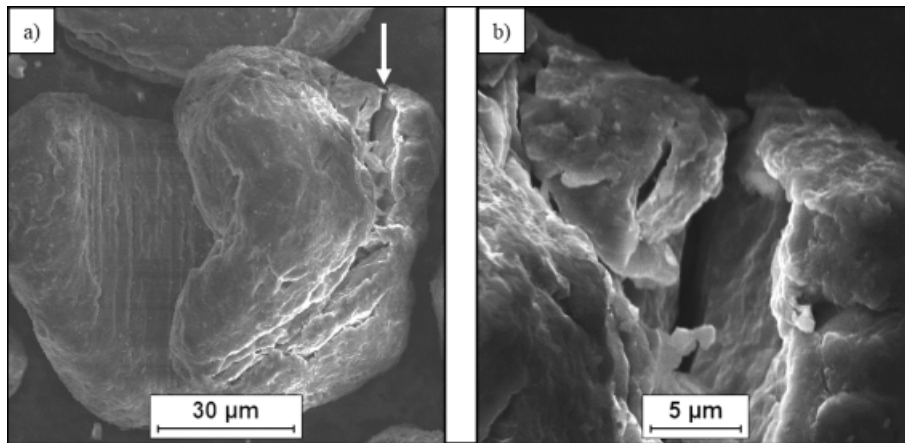
Fig. 3. SEM micrographs of magnesium powder after vertically-torsional vibration, decomposition of Mg particle by Mg-MgO scrap formation

metal-oxide scraps from magnesium particles can be observed (Fig. 3).

The obtained composite samples, 30 mm in diameter and 5 mm high, were cross-sectioned, and then the polished and non-etched samples were examined by light microscopy (Nikon Eclipse MA-200) and scanning electron microscopy (Hitachi S-4200 with EDS analyzer). The apparent density and open porosity were determined with the use of the Archimedes method. The Vickers microhardness was measured at the composite cross-sections by means of the Duramin-5 hardness testing machine under the load of 20 N, and it was determined in 5 regions (5 measurements each) from the sample's top to bottom.

Due to the microscopic observation results showing differences in the magnesium matrix microstructure, the image analysis was carried out with the use of light microscopy images for 20 areas registered from the composite sample cross-sections, in two zones at the top (10 areas) and the bottom (10 areas). That method was used to characterize the stereological parameters of the MgO phase, because the presence of an oxide film on the initial magnesium powder surface and its further mechanical degradation are inevitable in the applied technology and may influence the final material properties. The image conversion before the quantitative evaluation consisted of shadow correction, automatic binarization (k-means) and finally, binary image correction by a single opening. An example of that procedure is shown in Fig. 4.

3. Results and discussion

The light microscopy observations show (Fig. 5) that the phenomenon of carbon foam (black, irregular areas) penetration by magnesium successfully occurred. Additionally, in the matrix, elongated and slightly curved (flake-like in 3D), ring-like, or globular phases (Fig. 5d) were observed, with similar thickness or diameter of a few micrometers. This effect suggests that the oxide elements originate from the surface of the initial magnesium powder grains. Beside the morphology, the color of these phases (grey) was different compared to the applied carbon foams (black) or magnesium (light). In the composite reinforced with $C_{of}20$, their accumulation in the bottom region of the fabricated sample was observed, and a ring-like shape was very frequent (Fig. 5a and b). A roller of the composite reinforced with $C_{of}80$ also exhibits the accumulation of a grey phase, a few micrometers thick, in the bottom region, but with the dominance of elongated phases (flake-like in 3D, Fig. 5d). The main difference was observed in the top region; the oxides were globular and located near the carbon foam (Fig. 5a) or elongated with the absence of ring-like phases (Fig. 5c).

The observation results showed that, during the mechanical compaction, beside the abrasion which occurred among the Mg powder grains as well as between the Mg particles and the carbon foam, the micro-cutting process (Fig. 2b) at the sharp edges of the foam windows took place. Due to that process,
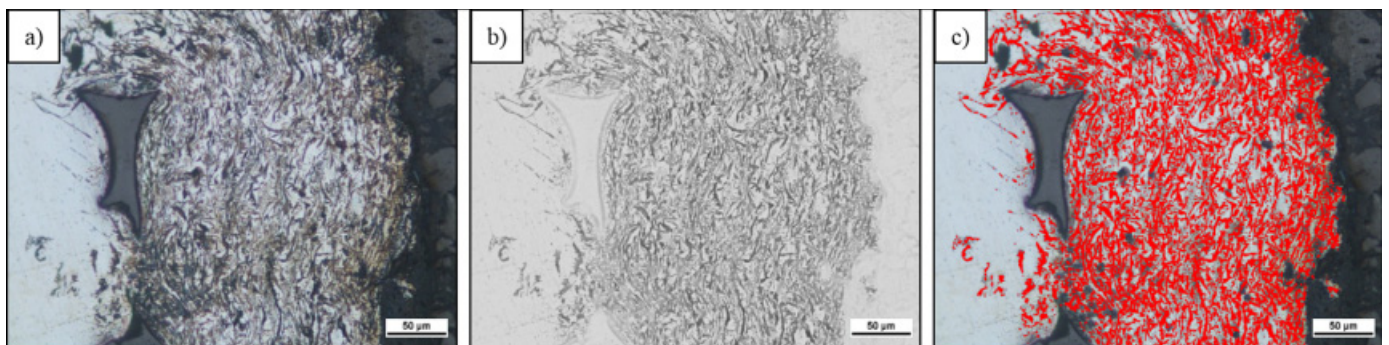

Fig. 4. LM image transformation of C_{of}-Mg composite micrograph for MgO quantitative evaluation: a) initial LM image, b) shadow correction 8, c) automatic binarization (k-means) and opening-1 correction
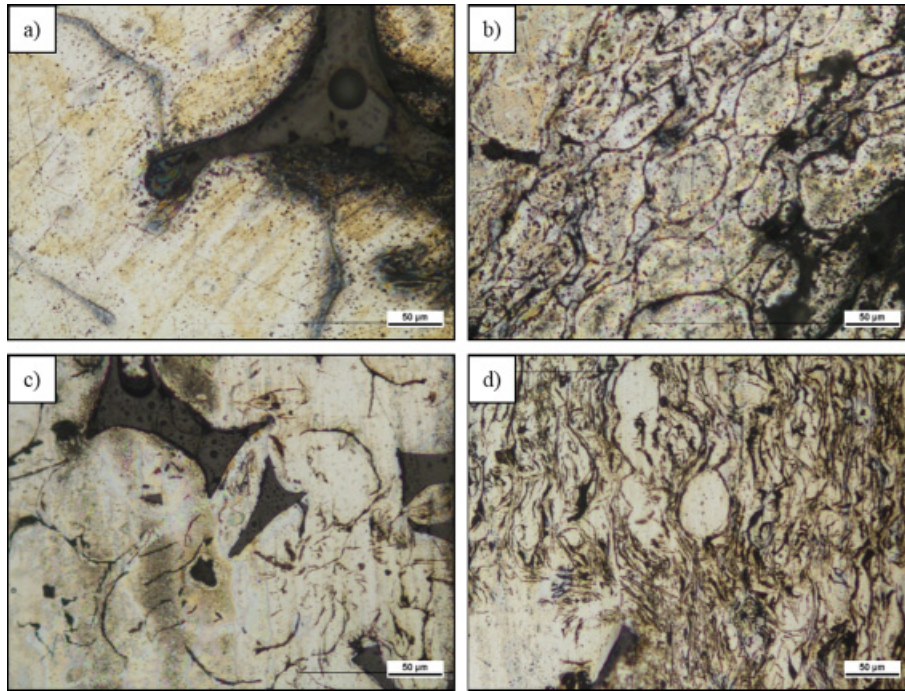
Fig. 5. LM micrographs of the obtained composites microstructure: $C_{of}20$-Mg (a,b) and $C_{of}80$-Mg (c,d), top regions (a,c), bottom regions (b,d)

decomposed oxides layers partially connected with a thin metal layer were forming (Fig. 3b) and then, after the hot pressing, the oxides were surrounded by the magnesium matrix (Fig. 5). Otherwise, the agglomerates of parallel elongated oxides with pores between can be dominant in the microstructure because the sintering process of MgO is ineffective with the applied hot pressing parameters. The accumulation of ring-like oxides in the bottom zone of the composite sample can be induced by an easier transportation of the finest Mg particles through the foam windows, without effective oxide film degradation.

The SEM examinations with the EDS analysis showed that all the thin, elongated and ring-like phases, as well as very fine globular phases, contain oxygen, which confirmed their expected oxide character (Fig. 6, 7). The presence of a few micropores

was detected, mainly near the carbon foam and in the microareas of the oxide agglomeration.

The image analysis was carried out with the use of light microscopy images, and oxide phases were detected. Their examples after binarization and correction for both composites in the top and bottom zones are shown in Fig. 8, while the quantitative metallography results are presented in Table 2.

The quantitative evaluation shows (Tab. 2) some differences between the composites with different glassy carbon foam cell sizes. For the $C_{of}80$-Mg composite with the carbon cell size lower (80 ppi, ~350 µm) than that in the $C_{of}20$-Mg composite (20 ppi, ~800 µm), the area fraction of the oxides A_A is higher in the same region and the mean particle oxide plane section is higher. However, there were also some similarities: in the top regions,
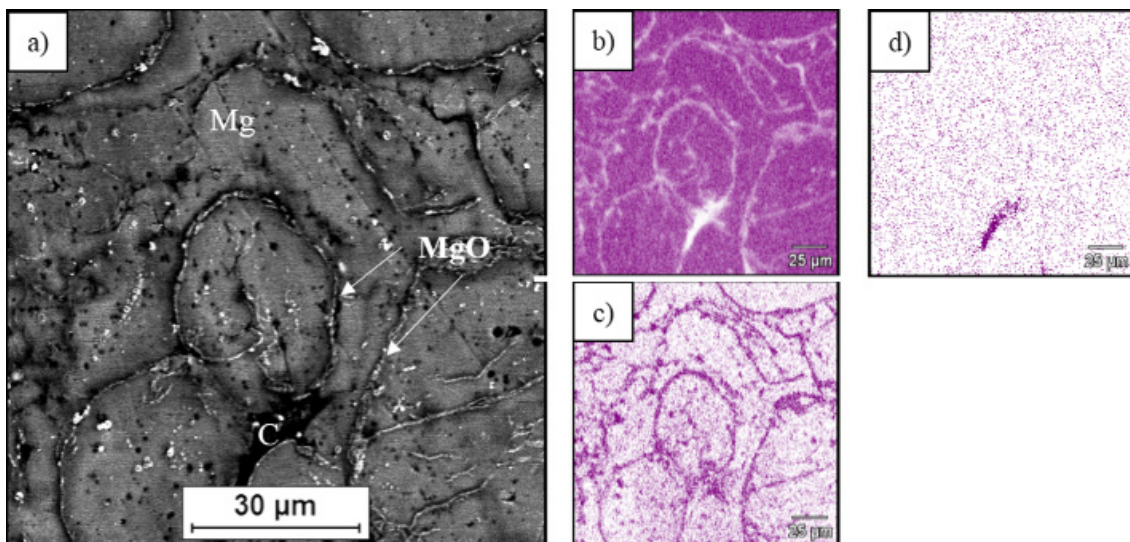

Fig. 6. SEM micrograph of $C_{of}20$-Mg composite sample in middle region (a) with X-ray mapping of Mg (b), O (c) and C (d)
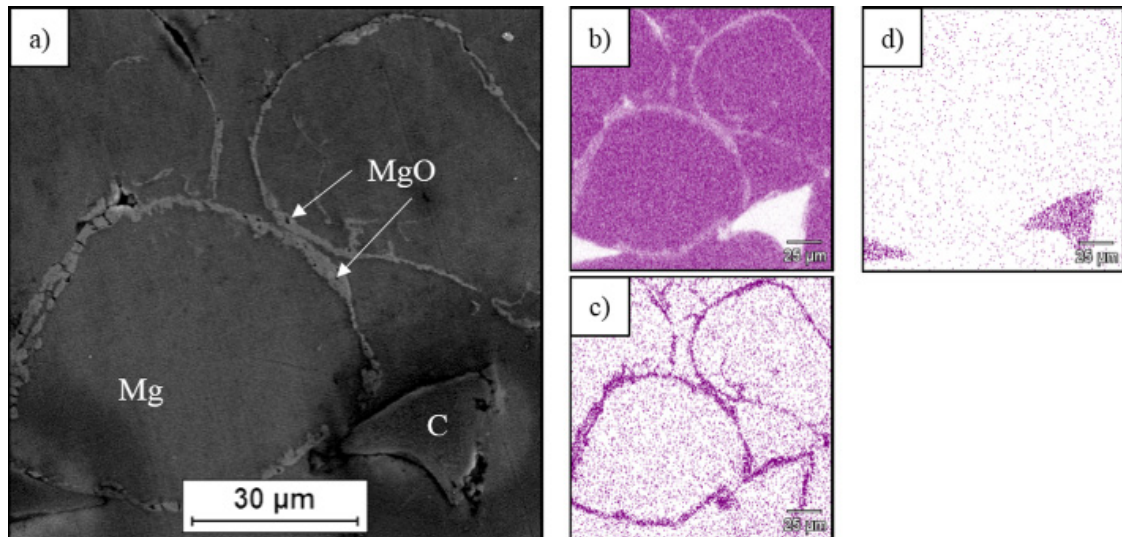
Fig. 7. SEM micrograph of a $C_{of}80$-Mg composite sample in middle region (a) with X-ray mapping of Mg (b), O (c) and C (d)
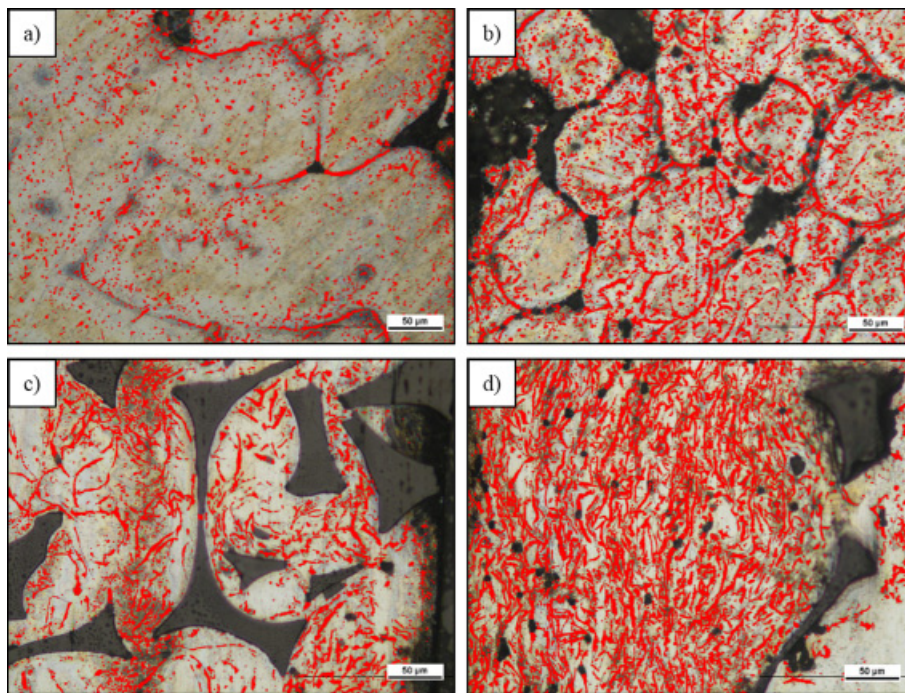

Fig. 8. LM images with an oxide phase detected in composites: $C_{of}20$-Mg (a, b) and $C_{of}80$-Mg (c, d), top regions (a, c) and bottom regions (b, d)

TABLE 2

Quantitative evaluation of oxides in top and bottom areas of the fabricated composites

Parameter	$C_{of}20$-Mg composite		$C_{of}80$-Mg composite	
	Top	Bottom	Top	Bottom
Area fraction of oxides A_A; %	2.72±0.4	5±1.02	3.14±0.89	7.01±0.9
Mean area of oxide particle plane section A; μm^2	5.74±0.59	11.10±1.77	11.36±0.99	23.44±2.57
Dimensionless shape factor ξ	0.92±0.01	0.89±0.01	0.86±0.01	0.79±0.01
Dimensionless elongation factor δ	1.57±0.02	1.60±0.01	1.76±0.03	1.91±0.04

the area fraction of the oxides as well as the mean values of the oxide particle area plane section A were always lower than in the bottom. In the case of the dimensionless shape factor ξ, its value in the top region is higher and for the dimensionless elongation factor δ, the value is lower. This suggests a tendency for the accumulation of elongated (flake-like) oxides in the bottom region, while the migration of the finest globular particles is less effective, which was earlier confirmed in the microscopic observations (Fig. 5). It must be mentioned that the effect is stronger for a lower cell size – a higher ppi value ($C_{of}80$-Mg composite).

The obtained results of the microscopic examinations combined with quantitative metallography can be explained by the conditions of the magnesium powder consolidation in the open-celled foam: the hard and sharp window edges (Fig. 1b, c) work as cutting micro-tools. The intensity of the micro-cutting effect is dependent on the foam geometry, because, for the applied carbon foams of different cell sizes but the similar porosity and cell/window size ratio, the total length of the window edges increases with the cell size decrease.

The results of the apparent density, open porosity and microhardness measurements are presented in Table 3. The low apparent density of both sinters, in comparison with the bulk components, indicates that the porosity of the composites is high, particularly for the $C_{of}20$-Mg composite, which is twice as high as that of $C_{of}80$-Mg. However, the mean microhardness (25 measurements in the cross-sectioned sample) of $C_{of}20$-Mg was lower and showed a lower standard deviation than that of the other composite. That result can be explained by the analysis of the microhardness change across the sample, measured from the top to the bottom, presented in Figure 9.

The linear distribution of microhardness showed differences between the 5 examined zones (mean value of 5 measurements in each zone). The microhardness obtained for the top zone decreases in the middle-top zone and then increases, and receives values which are a dozen percent higher for $C_{of}20$-Mg and several dozen percent higher for $C_{of}80$-Mg in the bottom zone. The results for the middle-top zone can be explained by the pores' accumulation in this region, but the further hardness value increase is a result of a change of the matrix properties.

TABLE 3

Density, porosity and Vickers microhardness of C_{of}-Mg composites

Material	Apparent density [g/cm³]	Open porosity [%]	Microhardness [HV2]
$C_{of}20$-Mg	1.43±0.001	22.58±0.03	50.9±4.5
$C_{of}80$-Mg	1.64±0.001	9.76±0.05	42.0±9.5

The observed effect was possible due to the presence of oxides and their proper connection with the metal matrix after melting and pressing.

The composite elements obtained by the proposed powder metallurgy method were characterized by relatively high open porosity and different microstructures at the cross-section, and one may question their potential usability. It seems that the high chemical stability of glassy carbon and the poor chemical resistance of magnesium in contact with the human body make that composite a good candidate as a biomaterial. Both components are well-known separately in different medical applications – magnesium and its alloys in the form of implants [33-34], and carbon in the form of implants or protective layers [16,35]. In the interpenetrating composite system C_{of}-Mg, selective corrosion of the composite elements can be expected, but first, laboratory examinations in physiological liquids are necessary. We can anticipate the process of tissue in-growth into the carbon open-celled foam in the exhibited new material, after the magnesium absorption by the human body. At first, the glassy carbon will be a reinforcing element of the magnesium base composite and after prolonged magnesium absorption, the more stable glassy carbon will improve the bone regeneration process. Also, it can
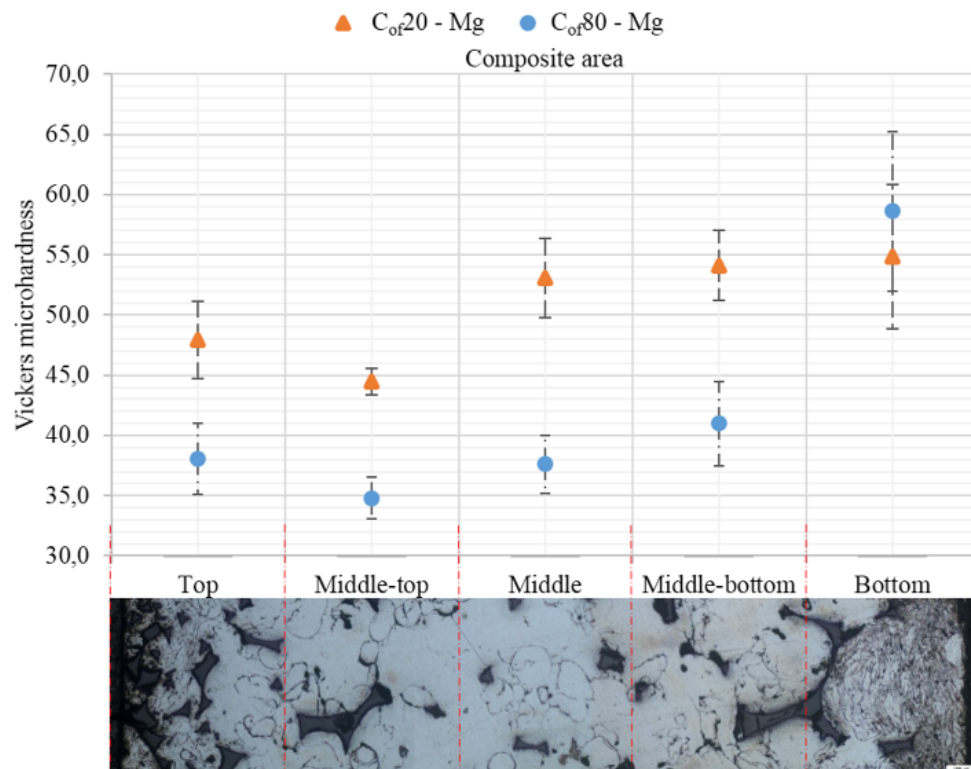

Fig. 9. Vickers microhardness changes in the cross-sectioned $C_{of}20$-Mg and $C_{of}80$-Mg composite elements and an example of the tested regions LM images

be anticipated that the presence of MgO in the composite will be suitable, because that compound is applied in biomedical materials for the improvement of the bone tissue in-growth [36-37].

4. Conclusions

A magnesium matrix composite reinforced with open-celled glassy-carbon foams was presented as a new ultralight material and a technique of its fabrication by powder metallurgy was characterized. The conclusions of the presented experiments are as follows:

1. The proposed foam-metal consolidation technique, including the magnesium powder particles' movement and compaction in the carbon foam cells by vertically-torsional vibration, was effective.

2. The vertically-torsional vibration caused the phenomenon of micro-cutting exerted by the hard and sharp edges of the open-celled foam windows, which occurs on the soft Mg powder surface coated with a thin MgO film. Owing to this, a few micrometer thick elements of different shapes are formed in the C_{of}-Mg system.

3. The hot pressing process, applied as the second step of the composite manufacture, causes enrichment of the magnesium matrix with dispersive MgO, but that magnesium microstructure change is dependent on the applied foam. For the similar foam porosity and cell/window size ratio, the amount and size of the oxides increases with the cell size decrease (higher ppi parameter).

4. Independently of the glassy-carbon foam cell size, in the bottom region of the obtained composite elements, a higher MgO content and microhardness were revealed.

5. The interpenetrating C_{of}-Mg composite containing conventional biomedical components, i.e., resistant to electrochemical corrosion, glassy-carbon open-celled foam and, non-toxic but easily corroding, magnesium matrix enriched with MgO particles, will undergo selective electrochemical corrosion in the environment of the human body, and that indicates implants as the potential application possibilities.

REFERENCES

[1] R. Daudin, S. Terzi, C. Mallmann, R.S. Martín, P. Lhuissier, E. Boller, Mater. Sci. Eng. A **688**, 76 (2017).

[2] W. Wle, M. Gupta, NanoWorld J. **2**, 78 (2017).

[3] G. Parande, V. Manakari, G.K. Meenashisundaram, M. Gupta, Int. J. Mater. Res. **107**, 1091 (2016).

[4] E.M. Salleh, H. Zuhailawati, S. Ramakrishnan, B.K. Dhindaw, Metall. Mater. Trans. A **48**, 2519 (2017).

[5] H. Hu, Scripta Mater. **39**, 1998.

[6] A. Olszówka-Myalska, J. Myalski, J. Chrapoński, Int. J. Mater. Res. **106**, 741 (2015).

[7] A. Olszówka-Myalska, J. Myalski, Solid State Phenom. **229**, 115 (2015).

[8] W. Hufenbach, M. Andrich, A. Langkamp, A. Czulak, J. Mater. Process. Technol. **175**, 218 (2006).

[9] C.S. Goh, J. Wei, L.C. Lee, M. Gupta, Nanotechnology **17**, 7 (2006).

[10] K.N. Braszczyńska-Malik, E. Przełożyńska, Inżynieria Materiałowa/Materials Engineering **211**, 115 (2016).

[11] A. Olszówka-Myalska, Solid State Phenom. **246**, 163 (2016).

[12] A. Olszówka-Myalska, S.A. McDonald, P.J. Withers, H. Myalska, G. Moskal, Solid State Phenom. **191**, 189 (2012).

[13] M. Inagaki, J. Qiu, Q. Guo, Carbon **87**, 128 (2015).

[14] R. Mehta, D.P. Anderson, J.W. Hager, Carbon **41**, 2174 (2003).

[15] M. Calvo, R. García, S.R. Moinelo, Energ. Fuel **22**, 3376 (2008).

[16] M.K. Pec, R. Reyes, E. Sánchez, D. Carballar, A. Delgado, J. Santamaría, M. Arruebo, C. Evora, Eur. Cells Mater. **20**, 282 (2010).

[17] Z. Nowak, M. Nowak, R.B. Pęcherski, M. Potoczek, R.E. Śliwa, Arch. Metall. Mater. **60**, 1957 (2015).

[18] M. Potoczek, A. Zima, Z. Paszkiewicz, A. Ślosarczyk, Ceram. Int. **35**, 2249 (2009).

[19] J. Myalski, B. Hekner, A. Posmyk, Tribologia **5**, 89 (2015).

[20] S. Vaucher, J. Kuebler, O. Beffort, L. Biasetto, F. Zordan, P. Colombo, Key Eng. Mater. **68**, 3202 (2008).

[21] W. Jiejun, L. Chenggong, W. Dianbin, G. Manchang, Key Eng. Mater. **63**, 569 (2003).

[22] A.J. Dolata, Materials **10**, 1045 (2017).

[23] M. Kremzer, M. Dziekońska, M. Sroka, B. Tomiczek, Arch. Metall. Mater. **61**, 1255 (2016).

[24] A. Mattern, B. Huchler, D. Staudenecker, R. Oberacker, A. Nagel, M.J. Hoffman, J. Eur. Cer. Soc. **24**, 3399 (2004).

[25] M.R. Nangrejo, X. Bao, M.J. Edirisinghe, J. Eur. Cer. Soc. **20**, 1777 (2000).

[26] M.I. Pech-Canul, R.N. Katz, M.M. Makhlouf, S. Pickard, J. Mater. Sci. **35**, 2169 (2000).

[27] B.S. Rao, V. Jarayam, Acta Mater. **49**, 2373 (2001).

[28] S. Elmori, R. Boukhili, C. San Marchi, A. Mortensen, D.J. Lloyd, J. Mater. Sci. **32**, 2131 (1997).

[29] M. Thünemann, O. Beffort, S. Kleiner, U. Vogt, Comp. Sci. Tech. **67**, 2377 (2007).

[30] K. Konopka, M. Szafran, J. Mater. Process. Tech. **175**, 266 (2006).

[31] J. Michalski, T. Wejrzanowski, S. Gierlotka, J. Bieliński, K. Konopka, T. Kosmac, K.J. Kudrzyłowski, J. Eur. Cer. Soc. **27**, 831 (2007).

[32] Patent application No. P.422259, A. Olszówka-Myalska, J. Myalski, M. Godzierz.

[33] G. Xue-Nan, L. Shuang-Shuang, L. Xiao-Ming, F. Yu-Bo, Front. Mater. Sc. **8**, 200 (2014).

[34] D. Wenjiang, Regen Biomater. **3**, 79 (2016).

[35] N. Saito, K. Aoki, Y. Usui, M. Shimizu, K. Hara, N. Narita, N. Ogihara, K. Nakamura, N. Ishigaki, H. Kato, H. Haniu, S. Taruta, Y.A. Kim, M. Endo, Chem. Soc. Rev. **40**, 3824 (2011).

[36] B.S. Necula, L.E. Fratila-Apachitei, A. Berkani, I. Apachitei, J. Duszczyk, J. Mater. Sci.: Mater. Med. **20**, 339 (2009).

[37] S.Z. Khalajabadi, M.R.A. Kadir, S. Izman, R. Ebrahimi-Kahrizsangi, Mater. Design **88**, 1223 (2015).